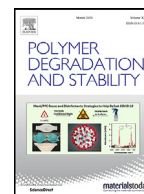




Contents lists available at ScienceDirect

Polymer Degradation and Stability

journal homepage: www.elsevier.com/locate/polymdegradstab

Effects of accelerated aging on thermal, mechanical, and shape memory properties of a cyanate-based shape memory polymer: II atomic oxygen

Fang Xie^a, Xiaobo Gong^a, Longnan Huang^b, Liwu Liu^c, Jinsong Leng^d, Yanju Liu^{c,*}^a School of Ocean Engineering, Harbin Institute of Technology, Weihai 264209, China^b Department of Materials Science and Engineering, Harbin Institute of Technology, Weihai 264209, China^c Department of Astronautical Science and Mechanics, Harbin Institute of Technology, Harbin 150001, China^d Center for Composite Materials and Structures, Harbin Institute of Technology, Harbin 150080, China

ARTICLE INFO

Article history:

Received 24 November 2020

Revised 23 January 2021

Accepted 3 February 2021

Available online 6 February 2021

Keywords:

Cyanate resin

Atomic oxygen

Shape memory effect

Thermal properties

Mechanical properties

Space environment

ABSTRACT

As a new kind of smart material with shape changing and fixing abilities, the shape memory polymer (SMP), has become a research hotspot for space deployment structures in recent years. In fact, studying the space environmental adaptability of SMPs is an urgent research task, promoting their application in the aerospace field. In this study, a chemical crosslinked cyanate-based SMP ($T_g \sim 206^\circ\text{C}$) was exposed to atomic oxygen in a ground simulation system. The irradiation effects of atomic oxygen were investigated in terms of microscopic morphology, chemical structure, thermal stability, mechanical properties, loss factor and the storage modulus. After exposure to atomic oxygen, the cyanate-based SMP showed obvious surface erosion. When the irradiation dose reached 10^{22} atoms/cm², the surface was entirely peeled off, and a new uneven surface emerged. However, the damage resulting from erosion was only on the surface and had little effect on the mechanical performance or shape memory behavior. The tensile strength and elastic modulus remained nearly constant at 66 MPa and 2000 MPa, respectively. Further, the effect of sample thickness and depth of delamination should be comprehensively considered in practical applications. The shape memory properties remain excellent after atomic oxygen irradiation, and the average shape fixity and shape recovery rates were 98.2% and 99.3%, respectively.

© 2021 Elsevier Ltd. All rights reserved.

Introduction

Shape memory polymers (SMP) are a new kind of intelligent polymer material that can change their shape from a certain temporary state (an interim state) back to their original state (a permanent state) under external excitation [1–3]. Due to its excellent shape memory effect (SME), SMPs have found their way in the field of spatially deployable structures [4–6]. The SMP-based spatial deployable structure can be folded on the ground and locked into a small temporary shape. Furthermore, it can deploy and recover to its original deployed shape under a suitable excitation when it enters the service orbit. Spacecraft in orbit must inevitably withstand the effects of harsh radiation environments, such as vacuum, heat, solar ultraviolet (UV) radiation, charged particle radiation, atomic oxygen (AO), and geomagnetic fields [7–9]. The harsh space environment can cause on-orbit damage to spacecraft mate-

rials and structures [10,11]. Therefore, the materials used in spacecraft structures must undergo rigorous space environmental reliability tests prior to application.

The density of AO is not high in a low earth orbit environment, and its effect can be ignored in static conditions. However, for a spacecraft to fly along an orbit at a speed of about 8 km/s, the beam density of AO impact must be approximately 10^{13} – 10^{15} atoms/(s•cm²). At such a high impact velocity, the average impact energy of AO is about 5 eV [12], which is enough to break chemical bonds in polymer materials. Due to powerful oxidizing properties, AO will cause oxidative erosion on the surface of exposed elements, which causes mass loss and performance degradation [13]. The oxidative erosion effect of AO also initiates gas volatiles from organic materials. The volatiles condensate on the surface of optical instruments and other equipment on satellites, causing sharp declines in their optical performance [14–16]. Flight experiments, long-term exposure experiments, and limited-term selective exposure experiments have confirmed that AO is one of the leading causes of material performance changes [17–19]. Therefore, the influence of AO on exposed materials in the space en-

* Corresponding author.

E-mail address: yj_liu@hit.edu.cn (Y. Liu).

environment require serious consideration. Several studies have focused on the performance of polyimide films exposed to the low earth orbit AO environment, and the AO flux is generally lower than 3.0×10^{21} atoms/cm² [19–23]. However, there are few reports on the spatial environmental adaptability of cyanate-based SMPs. Cyanate-based SMPs have become critical aerospace candidates due to their excellent high-temperature resistance [24] and dielectric properties [25]. In fact, they have been used to make a variety of space deployable structures, like thin and light mirrors [26,27]. In our previous work, a series of cyanate-based SMPs were studied using bisphenol A cyanate ester and two different modifiers, polyethylene glycol and polybutadiene-acrylonitrile. This material system had an adjustable T_g (up to 255°C) and good shape memory performance [28]. Its UV radiation resistance has been studied in a simulated space UV irradiation environment. The results show few significant changes in thermal-mechanical properties and shape memory properties before and after UV irradiation, indicating that they have excellent UV resistance [29]. In this work, we further investigate the performance of cyanate-based SMPs exposed to up to 10^{22} atoms/cm² of AO. The effects of the AO environment on the microstructure, chemical composition, mechanical properties, thermal stability, and shape memory properties of the cyanate-based SMPs are discussed. The AO fluence of the polyimide films exposed to all components of the LEO environment on the Materials International Space Station Experiment (MISSE) platform MISSE-1 was $\sim 8 \times 10^{21}$ atoms/cm². The flight experiment of MISSE-1 was retrieved after 3.9 years [21]. It can be calculated that the AO fluence of our work is probably equivalent to the cumulative dose of 5 years LEO flight.

Experimental

Materials and preparation methods

Bisphenol A cyanate monomer was supplied by JiangduWuqiao Resin Factory (China). Polyethylene glycol was provided by Tianjin Guangfu Fine Chemical Research Institute (China). All reagents were used as received. Firstly, cyanate monomer and polyethylene glycol were heated to melting, separately, and then, the two components were mixed under stirring. To obtain a prepolymer without air bubbles, the mixture was placed in a vacuum furnace to degas for 15 minutes. The degassed prepolymer was injected into a mold consisting of two flat plates separated by silica gel strips for curing. The curing process requires holding at 120°C for 2 hours, curing at 180°C for 2 hours, and curing at 210°C for 5 hours. The polyethylene glycol content was 28.6 wt%. Finally, a flat plate sample with a thickness of 2 mm was obtained.

AO exposure test

AO radiation environment experiments were performed using an AO environment ground simulation system at Beijing Institute of Spacecraft Environment Engineering, China. First, 5 eV of AO energy with a 5×10^{15} atoms/cm²·s flux under 6.0×10^{-2} Pa of pressure were used in the accelerated test. The accumulated doses of AO irradiation were 0, 3×10^{21} , 6×10^{21} , and 10^{22} atoms/cm² for specimens SMCR-0, SMCR-1, SMCR-2, and SMCR-3, respectively.

Characterization method

The surface morphology of the cyanate-based SMP was characterized by field-emission scanning electron microscopy (SEM; Quanta 200FEG, FEI Corporation, US) under an acceleration voltage of 30 kV.

The Fourier Transform infrared spectroscopy (FTIR) were recorded with a SPECTRUM ONE spectrometer (Perkin Elmer Cor-



Fig. 1. Images of cyanate-based SMP samples before and after AO irradiation.

poration, US) over a scan range of 4000–650 cm⁻¹ with a 4 cm⁻¹ resolution and scan times of 8. The FTIR sample was scraped from the exposed surface and prepared by the KBr disk method.

Thermogravimetric (TG) analysis was conducted on a TGA/DSC1 analyzer (Mettler-Toledo, Switzerland). The test sample used in the experiment was a powder, scraped from the exposed surface, with a total sample mass of 8–10 mg. The test was carried out at a heating rate of 10°C/min in a flowing nitrogen atmosphere, over a temperature range of 25 to 800°C.

The storage modulus and tan δ of the samples were studied by dynamic mechanical analysis (DMA; Q800, TA Corporation, US) in a tensile mode, heating from 25°C to 350°C by 3°C/min. All runs were performed at an amplitude of 10 μ m, frequency of 1 Hz, and minimum dynamic force of 0.1 N. Samples were shaped by a high speed engraving machine to dimensions of 20 \times 3 \times 1 mm³.

The quasi-static tensile test was performed on a Zwick/Roell Z010 tensile testing machine (Zwick GmbH & Co. KG) with an extensometer. The ambient temperature was 25°C, and the beam moving speed was 5 mm/min. The tensile test piece was cut from a polymer plate by a high-speed precision engraving machine, and the size of the test piece was in accordance with standard ASTM D638, Type IV.

The shape memory performance of cyanate-based SMP samples before and after AO irradiation was investigated using DMA (DMA Q800, TA Corporation, US). The test was carried out in force-controlled three-point bending mode. Real-time force, deflection (displacement of the midpoint), and temperature were recorded throughout the process. For the Nth cycle, the initial displacement of the sample was defined as D_{n0} . The sample was first bent at 210°C, with a force of 0.1 N, and the deflection was recorded as D_{n1} . Then, external force was removed when the sample fully cooled to room temperature, and the displacement value was recorded as D_{n2} . The temperature was increased to 210°C again to obtain the recovered shape, and the displacement was recorded as $D_{(n+1)0}$, that is, the initial displacement of the (N+1)th cycle. The shape fixation rate, R_{nf} , and the shape recovery rate, R_{nr} , of the Nth cycle can be expressed as [29]:

$$R_{nf} = \frac{D_{n2} - D_{n0}}{D_{n1} - D_{n0}} \times 100\% \quad (1)$$

$$R_{nr} = \frac{D_{n2} - D_{(n+1)0}}{D_{n2} - D_{n0}} \times 100\% \quad (2)$$

Results and discussion

Morphology and chemical structure

Fig. 1 is a comparison photograph of the cyanate-based SMP samples before and after AO irradiation, and it shows that as the

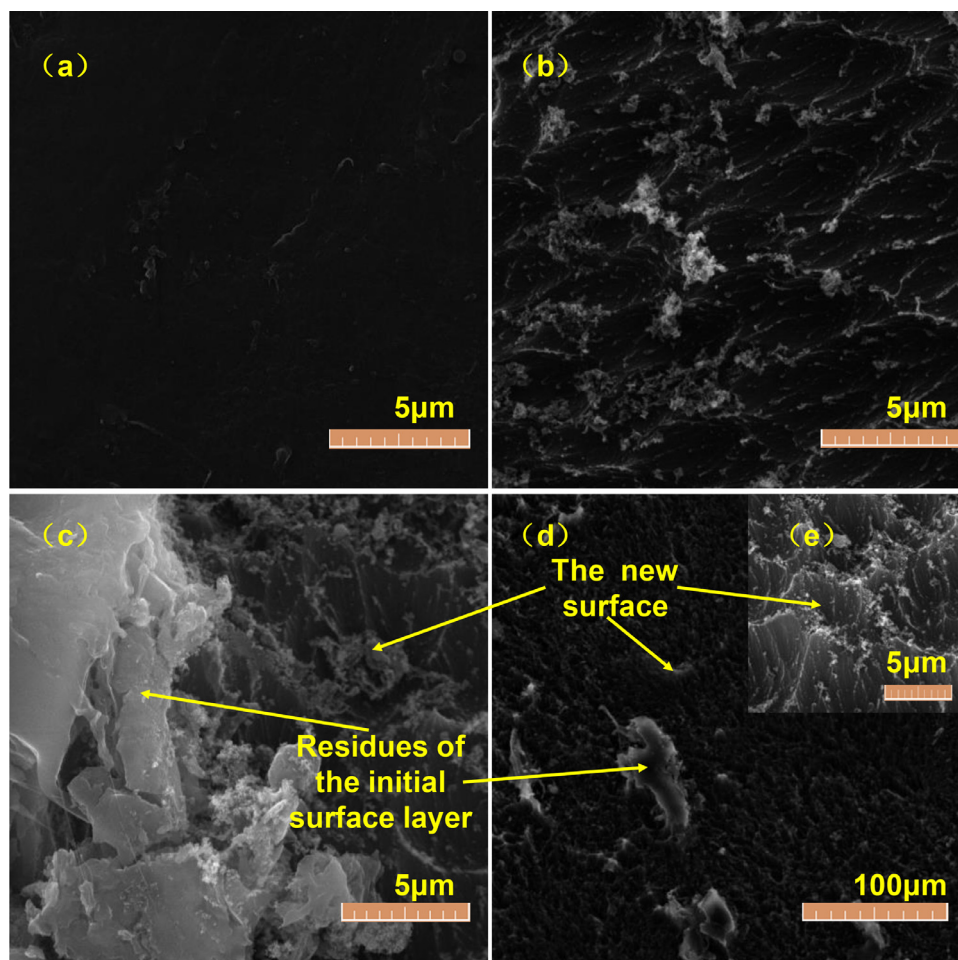


Fig. 2. Micromorphology of cyanate-based SMP before and after AO irradiation. (a) before exposure to AO (SMCR-0), (b) after exposure to 3×10^{21} atoms/cm² of AO radiation (SMCR-1), (c) after exposure to 6×10^{21} atoms/cm² of AO radiation (SMCR-2), and (d–e) after exposure to 10×10^{21} atoms/cm² of AO radiation (SMCR-3).

total flux of AO irradiation increases, opaque, whitish, and rough structures gradually emerged on the sample surface.

Morphology of cyanate-based SMP exposed to AO radiation was observed by field-emission SEM. The SEM image shows that before exposure to AO radiation, the surface of SMCR-0 was flat and smooth (see Fig. 2(a)). After exposure to 3×10^{21} atoms/cm² of AO radiation, the surface of SMCR-1 became rough and dense, and tiny grooves less than 1 μm deep appeared on it (Fig. 2(b)). Erosion increased with increasing AO irradiation dose. When the radiation dose reached 6×10^{21} atoms/cm², part of the sample surface layer was exfoliated. The right area of Fig. 2(c) shows a new surface after serious erosion, and the left area shows some initial surface layer residues, weakly attached to the sample. The erosion depth reached about 3 μm. When the radiation dose reached 10×10^{21} atoms/cm², the erosion depth was about 5–20 μm and the surface layer peeled off almost entirely, and the new surface (Fig. 2(e) and the dark area of Fig. 2(d)) was uneven. Microscopic analysis indicated that the main manifestations of AO erosion of cyanate-based SMPs were increased roughness, grooves, plaques, and exfoliation of the surface layer, consistent with previous research [30].

Changes in specific chemical functional groups were analyzed by infrared spectroscopy. The infrared spectra of cyanate-based SMP samples before and after exposure to AO are shown in Fig. 3. Specifically, Figs. 3a, b, c, and d correspond to samples SMCR-0, SMCR-1, SMCR-2, and SMCR-3, respectively. We know that the cyanate monomer undergoes trimerization during the curing process to form a three-dimensional network structure dominated by six-membered oxygen-linked triazine rings [31]. Characteris-

tic peaks for the triazine rings are located at $1510\text{--}1560\text{ cm}^{-1}$ and 1356 cm^{-1} [32–34]. As seen in Fig. 3, the characteristic peaks of the triazine ring do not change significantly after AO exposure. This is mainly due to the high bond energy of the triazine rings, which is over 2000 kJ/mol. However, the exposed samples show new bands in the stretching (3211 cm^{-1}) [35] and bending (1465 cm^{-1} , 1423 cm^{-1} , and 1403 cm^{-1}) vibration regions of the methyl C–H and hydroxyl O–H bonds. The new methyl C–H bond is attributed to the breaking of the polyethylene glycol chain under the attack of high-energy AO. The new hydroxyl O–H bond could be attributed to intercalation of AO between the carbon and hydrogen atoms, resulting in alcoholic or phenolic hydroxyl groups.

In addition, two new characteristic peaks appeared around 1710 cm^{-1} and 1780 cm^{-1} , corresponding to the carbonyl C=O stretching vibration of carboxylic acids or esters [36]. As the samples were exposed to a large number of oxygen atoms, the high-energy oxygen atoms could not only attack the chemical bonds but also quickly combine with carbon atoms at the break in the chain to form carbon-oxygen double bonds, resulting in these new peaks. In the UV exposure test [29], the peak of C=O was much more striking when the exposure time reached 3000 ESH compared to 1000 ESH and 2000 ESH. In contrast, a striking C=O peak appeared with low flux AO irradiation (3×10^{21} atoms/cm²). This feature was attributed to the high energy of AO, making it easy to break old bonds and form the new C=O bonds.

Therefore, the effect of AO exposure on the chemical structure of cyanate based SMP can be summarized as follows. Firstly, the

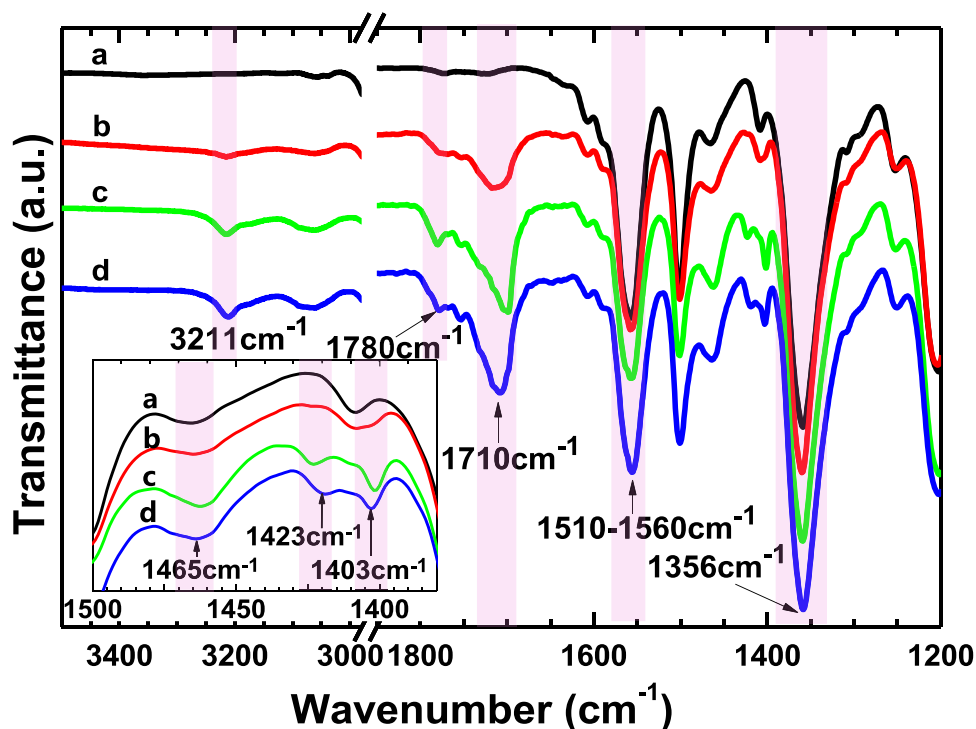


Fig. 3. FTIR spectra of cyanate-based SMPs before and after AO irradiation: (a) SMCR-0, (b) SMCR-1, (c) SMCR-2, and (d) SMCR-3.

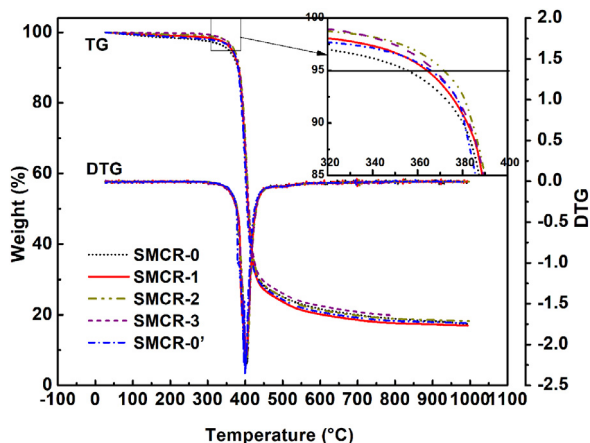


Fig. 4. TG curves of cyanate-based SMPs before and after AO irradiation.

sample surface was bombarded by high-energy AO. The benzene and triazine rings were unchanged, but some of the C-H and C-C bonds were broken. Soon, the oxygen atoms immediately participated in bond formation at the break, resulting in new C=O and O-H bonds. At the same time, high-energy AO directly led to physical peeling of the resin, resulting in increased roughness, grooves, plaques, and exfoliation of the surface layer, observed by SEM analysis.

Thermal stability

The TG curve of cyanate-based SMP before and after exposure to AO is shown in Fig. 4. The initial thermal decomposition temperature is defined as the temperature at which the mass loss of the sample reaches 5%. As shown in the figure, the initial thermal decomposition temperatures of SMCR-0, SMCR-1, SMCR-2, and SMCR-3 are 356°C, 364°C, 372°C, and 368°C, respectively. Similar to UV

irradiation [29], the initial decomposition temperature of the samples after AO exposure increased by 8°C, 16°C, and 12°C, respectively. The behavior occurred because there are unreacted small molecules or impurities (water absorbed in the air, carbon dioxide, etc.) in the cyanate-based SMP samples. These small molecules contained in the exposed samples (SMCR-1, SMCR-2, and SMCR-3) were expelled from the sample when exposed to AO in high vacuum. However, the small molecules contained in the unexposed sample (SMCR-0) were only released due to the gradual increase in temperature in the TG test. Therefore, the initial thermal decomposition temperatures of the exposed samples are higher than that of unexposed SMCR-0. To verify this speculation, a control sample, SMCR-0' were vacuum outgassed for 24 h before analyzing it by TG analysis. As shown in Fig. 4, the initial thermal decomposition temperature of SMCR-0' is 366°C, which is 10°C higher than SMCR-0 and at the same level of the exposed samples. It is further proved that the reason for the higher initial decomposition temperature of AO-exposed samples (SMCR-1, SMCR-2, and SMCR-3) is caused by the high vacuum, rather than the direct effect of AO exposure. The thermal decomposition rate is generally defined as the derivative of the thermogravimetric curve (DTG). As shown in the DTG curve, above the initial decomposition temperature, the sample weight began to decline sharply, and the thermal decomposition rate increased with the increasing temperature, reaching a maximum at 400°C.

The final carbon retention rate refers to the mass fraction of the remaining sample when the sample mass no longer decreases and gradually stabilizes to the original sample mass. Notably, the final carbon retention rates of SMCR-0, SMCR-1, SMCR-2, and SMCR-3 were 19%, 17.6%, 19%, and 19.5%, respectively, showing an initial decrease followed by an increase with an increase in AO exposure. This is because the original three-dimensional molecular structure of the residue that adhered to the sample surface after being bombarded by AO was destroyed, and its thermal stability deteriorated. When the surface of the sample was completely exfoliated, a fresh cyanate-based SMP surface with high thermal stability appeared, resulting in a gradual increase of the final carbon retention rate.

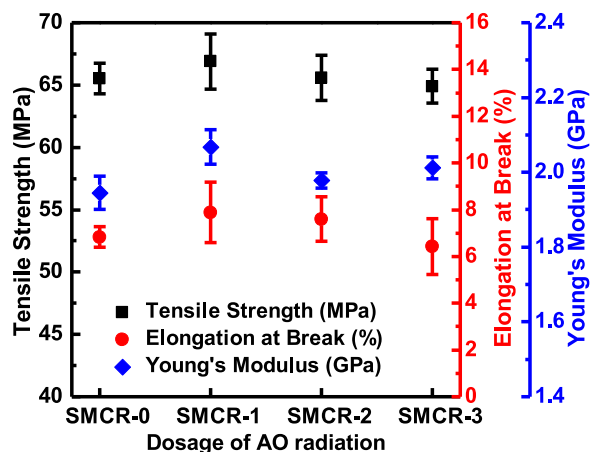


Fig. 5. Mechanical properties of cyanate-based SMPs before and after AO irradiation.

However, this change is relatively small, only within 2%, proving that the AO exposure test had little effect on the thermal stability of cyanate-based SMP samples.

Mechanical properties

The mechanical properties before and after exposure to AO under vacuum are shown in Fig. 5. The tensile strengths of SMCR-0, SMCR-1, SMCR-2, and SMCR-3 are all around 66 MPa (66 ± 1 , 67 ± 2 , 66 ± 2 , and 65 ± 1 MPa, respectively). The average strain at break of all samples were maintained between 6–8%, and the elastic moduli were all around 2000 MPa (1950 ± 40 , 2070 ± 50 , 1980 ± 20 , and 2010 ± 30 MPa). The sample thickness used in the mechanical test was 3 mm. Although the AO exposure experiment severely eroded the sample surface, it had little effect on the overall mechanical properties of the sample. Therefore, the scale of the original sample thickness and depth of ablation must be considered comprehensively to determine whether protection is required in practical use.

Dynamic thermomechanical properties

The dynamic thermomechanical curves of cyanate-based SMPs before and after exposure to AO are shown in Fig. 6. We see that the storage modulus curve of the sample has two stages: low temperature high modulus and high temperature low modulus. The storage modulus of the two stages differ by 2–3 orders of magnitude. This change in modulus manifests the viscoelasticity of the prepared cyanate-based SMP and also shows that this cyanate-

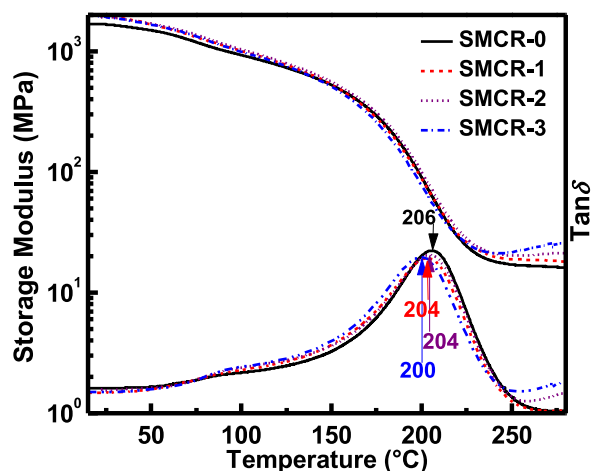


Fig. 6. DMA curves of cyanate-based SMPs before and after AO irradiation.

polyethylene glycol SMP system has network nodes (high temperature and low modulus to ensure that the material does not slip) and conversion segments (low temperature and high modulus to ensure that it is used as a structural material), which are key factors yielding its shape memory effect [37].

In addition, after exposure to 3×10^{21} , 6×10^{21} , and 10^{22} atoms/cm² of AO, the $\tan\delta$ curves did not change significantly, and the curve peaks only shifted to the lower temperature within 6°C. Moreover, as the AO dose increased, the storage modulus in the high temperature section (rubbery modulus) gradually increased, and the intensity of the $\tan\delta$ peak decreased. As the rubbery modulus of a thermoset system is proportional to its crosslink density [38–40], the increasing rubbery modulus and decreasing $\tan\delta$ peak intensity indicate that high-energy and high-density AO promotes a crosslinking reaction of cyanate-based SMP while ablating the surface of the material. This is thought to occur because AO is involved in bond formation, which is also indicated in the infrared analysis above.

Shape memory behavior

The shape memory processes of SMCR-0 and SMCR-3 Fig. 7) show that the sample was bent and deformed by applying a force of 0.1 N at 210°C (5°C above T_g), and the midpoint displacement of both samples were over 5 mm (span = 20 mm). R_{nf} and R_{nr} , calculated using Eqs. (1) and (2), of the two samples are shown in Table 1. It is evident that R_{nf} and R_{nr} of both SMCR-0 and SMCR-3 for the three shape memory cycles had good repeatability. The averages of R_{nf} and R_{nr} for the three shape memory cycles of SMCR-0

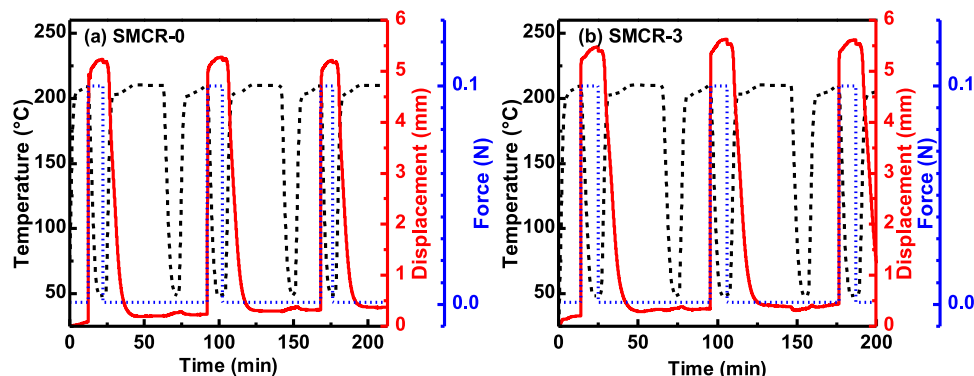


Fig. 7. The impact of AO radiation on the shape memory effect of cyanate-based SMPs: (a) SMCR-0 and (b) SMCR-3.

Table 1
 R_{nf} and R_{nr} of cyanate-based SMPs before and after AO irradiation.

Sample	N	1	2	3	Average
SMCR-0	R_{nf} (%)	97.8	97.9	97.1	97.6
	R_{nr} (%)	96.9	97.0	99.0	97.6
SMCR-3	R_{nf} (%)	98.3	98.2	98.2	98.2
	R_{nr} (%)	98.6	99.3	99.9	99.3

were both 97.6%, and those of SMCR-3 were 98.2% and 99.3%, respectively. Although the averages of R_{nf} and R_{nr} of SMCR-3 (after exposure to AO) improved by 0.6% and 1.7%, respectively, we believe that is in the error of the DMA measurement. Hence, these results indicate that the AO exposure experiment not only has no adverse effect on the shape memory performance of cyanate-based SMP.

Conclusion

In this study, the adaptability of the cyanate SMP to AO in the space environment was first studied by a ground simulation test. Specifically, cyanate-based SMP samples were exposed to AO at 0 , 3×10^{21} , 6×10^{21} , and 10^{22} atoms/cm². Following exposure to high-energy and high-density AO, the chemical bonds of the cyanate-based SMP were destroyed by bombardment, which was manifested as changes in chemical bonds and physical peeling of the surface resin. However, ablation was limited to the surface layer of the sample and had no adverse effects on the thermal stability, T_g , mechanical properties, and shape memory properties of the sample. We believe that when using cyanate-based SMPs in practice, the relative relationship between the sample thickness and ablation depth (corresponding to the service time in orbit) must be comprehensively considered. Under mild ablation, which does not affect the mechanical properties of the sample, the influence of AO may not be considered. However, if the service time in orbit is too long, the sample must be protected with an anti-AO film, like polyimide. In addition, the development of cyanate-based SMPs with intrinsic anti-AO properties is a promising research direction.

Declaration of Competing Interest

None.

Acknowledgements

This work was supported by the National Natural Science Foundation of China (Grant No. 11902099 & 11902100).

References

- [1] M. Behl, M.Y. Razaq, A. Lendlein, Multifunctional shape-memory polymers, *Advanced Materials* 22 (31) (2010) 3388–3410.
- [2] F. Xie, L. Huang, J. Leng, Y. Liu, Thermoset shape memory polymers and their composites, *Journal of Intelligent Material Systems and Structures* 27 (18) (2016) 2433–2455.
- [3] J. Leng, X. Lan, Y. Liu, S. Du, Shape-memory polymers and their composites: Stimulus methods and applications, *Progress in Materials Science* 56 (7) (2011) 1077–1135.
- [4] D. Zhang, L. Liu, J. Leng, Y. Liu, Ultra-light release device integrated with screen-printed heaters for CubeSat's deployable solar arrays, *Composite Structures* 232 (2020) 111561.
- [5] T. Liu, L. Liu, M. Yu, Q. Li, C. Zeng, X. Lan, Y. Liu, J. Leng, Integrative hinge based on shape memory polymer composites: Material, design, properties and application, *Composite Structures* 206 (2018) 164–176.
- [6] X. Lan, L. Liu, F. Zhang, Z. Liu, L. Wang, Q. Li, F. Peng, S. Hao, W. Dai, X. Wan, Y. Tang, M. Wang, Y. Hao, Y. Yang, C. Yang, Y. Liu, J. Leng, World's first space-flight on-orbit demonstration of a flexible solar array system based on shape memory polymer composites, *Science China Technological Sciences* 63 (8) (2020) 1436–1451.
- [7] A.L. Vampola, The hazardous space particle environment, *IEEE Transactions on Plasma Science* 28 (6) (2000) 1831–1839.
- [8] J. Chen, N. Ding, Z. Li, W. Wang, Organic polymer materials in the space environment, *Progress in Aerospace Sciences* 83 (2016) 37–56.
- [9] Y. Lu, Q. Shao, H. Yue, F. Yang, A Review of the Space Environment Effects on Spacecraft in Different Orbits, *IEEE Access* 7 (2019) 93473–93488.
- [10] S.D. Pearson, K.S. Clifton, NASA's Space Environments & Effects (SEE) Program: Contamination engineering technology development, in: P.T.C. Chen, Z.H. Gu, A.A. Maradudin (Eds.), *Rough Surface Scattering and Contamination* 1999, pp. 4–14.
- [11] J.L. Barth, Space and atmospheric environments: From low Earth orbits to deep space, 2003.
- [12] G.S. Arnold, D.R. Peplinski, Reaction of high-velocity atomic oxygen with carbon, *AIAA Journal* 24 (4) (1986) 673–677.
- [13] C. Chang, J.R. Tackett, Characterization of phenolic resins with thermogravimetry-mass spectrometry, *Thermochimica Acta* 192 (1) (1991) 181–190.
- [14] B.A. Banks, K.K. de Groh, S.K. Miller, Low earth orbital atomic oxygen interactions with spacecraft materials, in: M. Chipara, D.L. Edwards, R.S. Benson, S. Phillips (Eds.), *Materials for Space Applications*, Materials Research Society, Warrendale, 2005, pp. 331–342.
- [15] K.K. De Groh, B.A. Banks, C.E. McCarthy, R.N. Rucker, L.M. Roberts, L.A. Berger, MISSE 2 PEACE Polymers Atomic Oxygen Erosion Experiment on the International Space Station, *High Performance Polymers* 20 (4-5) (2008) 388–409.
- [16] J.A. Backus, B.A. Bank, K.K. de Groh, Atomic Oxygen Erosion Yield Predictive Tool for Spacecraft Polymers in Low Earth Orbit, 2008.
- [17] S. Tompkins, D. Bowles, S. Slemp, L. Teichman, Response of composite materials to the Space Station orbit environment, 29th Structures, Structural Dynamics and Materials Conference, American Institute of Aeronautics and Astronautics, 1988.
- [18] K.A. Trick, T.E. Saliba, Mechanisms of the pyrolysis of phenolic resin in a carbon/phenolic composite, *Carbon* 33 (11) (1995) 1509–1515.
- [19] H. Shimamura, T. Nakamura, Investigation of degradation mechanisms in mechanical properties of polyimide films exposed to a low earth orbit environment, *Polymer Degradation and Stability* 95 (1) (2010) 21–33.
- [20] M. Qian, V.J. Murray, W. Wei, B.C. Marshall, T.K. Minton, Resistance of POSS Polyimide Blends to Hyperthermal Atomic Oxygen Attack, *ACS Applied Materials & Interfaces* 8 (49) (2016) 33982–33992.
- [21] T.K. Minton, M.E. Wright, S.J. Tomczak, S.A. Marquez, L.H. Shen, A.L. Brunsvold, R. Cooper, J.M. Zhang, V. Vij, A.J. Guenther, B.J. Petteys, Atomic Oxygen Effects on POSS Polyimides in Low Earth Orbit, *ACS Applied Materials & Interfaces* 4 (2) (2012) 492–502.
- [22] N. Atar, E. Grossman, I. Gouzman, A. Bolker, V.J. Murray, B.C. Marshall, M. Qian, T.K. Minton, Y. Hanein, Atomic-Oxygen-Durable and Electrically-Conductive CNT-POSS-Polyimide Flexible Films for Space Applications, *ACS Applied Materials & Interfaces* 7 (22) (2015) 12047–12056.
- [23] U. Andropova, O. Serenko, N. Tebeneva, A. Tarasenkov, M. Buzin, E. Afanasyev, D. Sapozhnikov, S. Bukalov, L. Leites, R. Aysin, A. Polezhaev, A. Naumkin, L. Novikov, V. Chernik, E. Voronina, A. Muzafarov, Atomic oxygen erosion resistance of polyimides filled hybrid nanoparticles, *Polymer Testing* 84 (2020) 106404.
- [24] M.L. Ramirez, R. Walters, R.E. Lyon, E.P. Savitski, Thermal decomposition of cyanate ester resins, *Polymer Degradation and Stability* 78 (1) (2002) 73–82.
- [25] A. Kandelbauer, 11 - Cyanate Esters, in: H. Dodiuk, S.H. Goodman (Eds.), *Handbook of Thermoset Plastics*, William Andrew Publishing, Boston, 2014, pp. 425–457. Third Edition.
- [26] S.C. Arzberger, N.A. Munshi, M.S. Lake, J. Wintergerst, S. Varlese, M.P. Ulmer, W.A. Goodman (Ed.), Elastic memory composite technology for thin, lightweight space and ground-based deployable mirrors, *Optical Materials and Structures Technologies* (2003) 143–154 SPIE, San Diego, CA, United States.
- [27] S.C. Arzberger, M.L. Tupper, M.S. Lake, R. Barrett, K. Mallick, C. Hazelton, W. Francis, P.N. Keller, D. Campbell, S. Feucht, D. Codell, J. Wintergerst, L. Adams, J. Malliou, R. Denis, K. White, M. Long, N.A. Munshi, K. Gall, Elastic memory composites (EMC) for deployable industrial and commercial applications, in: E.V. White (Ed.), *Smart Structures and Materials 2005 - Industrial and Commercial Applications of Smart Structures Technologies*, San Diego, CA, United States, 2005, pp. 35–47. SPIE.
- [28] F. Xie, L. Huang, Y. Liu, J. Leng, Synthesis and characterization of high temperature cyanate-based shape memory polymers with functional polybutadiene/acrylonitrile, *Polymer* 55 (23) (2014) 5873–5879.
- [29] F. Xie, L. Liu, X. Gong, L. Huang, J. Leng, Y. Liu, Effects of accelerated aging on thermal, mechanical and shape memory properties of cyanate-based shape memory polymer: I vacuum ultraviolet radiation, *Polymer Degradation and Stability* 138 (2017) 91–97.
- [30] F. Awaja, J.B. Moon, S. Zhang, M. Gilbert, C.G. Kim, P.J. Pigram, Surface molecular degradation of 3D glass polymer composite under low earth orbit simulated space environment, *Polymer Degradation and Stability* 95 (6) (2010) 987–996.
- [31] E. Grigat, R. Pütter, Synthesis and Reactions of Cyanic Esters, *Angewandte Chemie International Edition in English* 6 (3) (1967) 206–218.
- [32] A. Osei Owusu, G.C. Martin, J.T. Gotro, Triazine formation in cyanate-based resin systems at room temperature conditions, *Polymer* 37 (21) (1996) 4869–4872.
- [33] J. Throckmorton, G. Palmese, Acceleration of cyanate ester trimerization by dicyanamide RTILs, *Polymer* 91 (2016) 7–13.

- [34] P. Bartolomeo, J.F. Chailan, J.L. Vernet, Curing of cyanate ester resin: a novel approach based on FTIR spectroscopy and comparison with other techniques, *European Polymer Journal* 37 (4) (2001) 659–670.
- [35] M.A. Corres, M. Zubitur, M. Cortazar, A. Múgica, Thermal and thermo-oxidative degradation of poly(hydroxy ether of bisphenol-A) studied by TGA/FTIR and TGA/MS, *Journal of Analytical and Applied Pyrolysis* 92 (2) (2011) 407–416.
- [36] F. Portillo, O. Yashchuk, É. Hermida, Evaluation of the rate of abiotic and biotic degradation of oxo-degradable polyethylene, *Polymer Testing* 53 (2016) 58–69.
- [37] T. Xie, Recent advances in polymer shape memory, *Polymer* 52 (22) (2011) 4985–5000.
- [38] A.M. Ortega, S.E. Kasprzak, C.M. Yakacki, J. Diani, A.R. Greenberg, K. Gall, Structure-property relationships in photopolymerizable polymer networks: Effect of composition on the crosslinked structure and resulting thermomechanical properties of a (meth)acrylate-based system, *Journal of Applied Polymer Science* 110 (3) (2008) 1559–1572.
- [39] C.M. Yakacki, T.D. Nguyen, R. Likos, R. Lamell, D. Guigou, K. Gall, Impact of shape-memory programming on mechanically-driven recovery in polymers, *Polymer* 52 (21) (2011) 4947–4954.
- [40] L.W. Hill, H.M. Korzeniowski, M. Ojunga-Andrew, R.C. Wilson, Accelerated clearcoat weathering studied by dynamic mechanical analysis, *Progress in Organic Coatings* 24 (1–4) (1994) 147–173.